TÜBİTAK

Turkish Journal of Earth Sciences

http://journals.tubitak.gov.tr/earth/

Research Article

Turkish J Earth Sci
(2023) 32: 306-319

doi:10.55730/1300-0985.1846

Identification of transtensional and transpressional features in the Sea of Marmara using onshore-offshore seismic and geodetic data

Zeynep COŞKUN*, Ali PINAR

Department of Earthquake Engineering, Kandilli Observatory and Earthquake Research Institute, Boğaziçi University, İstanbul, Turkey

Received: 01.04.2022 • **Accepted/Published Online:** 07.10.2022 • **Final Version:** 28.04.2023

Abstract: The scope of the study is to determine transtensional and transpressional features along the North Anatolian Fault beneath the Sea of Marmara, using seismic and geodetic data. For this purpose, focal mechanisms of small size NAF earthquakes, recorded by broadband stations and OBSs, have been derived and used as a tool to identify the transtensional and transpressional features. The focal mechanisms of: (1) small to moderate size events are obtained by the CMT inversion technique of Kuge (2003), using onshore waveform data from 2002–2015, (2) micro-earthquakes are obtained using the technique of Horiuchi (2015), using offshore waveform data recorded by 15 OBS stations from 2015–2016. Furthermore, published GPS velocities are used to determine the style of faulting and strain rates. The geodetic horizontal crustal strain rates are determined at equally spaced grid points by interpolating northing and easting components of the 112 GPS vectors from 1994–2013. The results indicate that extensional and strike-slip style deformation dominates the region, while contractional features are rare. Significant extension is observed in Çınarcık Basin and the area between Marmara Island and Central Basin. Yalova-Çınarcık region shows predominantly N-S extension while the Çınarcık Basin events show NE-SW extension. Compressional or transpressional features are derived to the west of Marmara Island and Ganos and in the Central segment extending from Central Basin toward Çınarcık Basin. The GPS strain rate results point out the highest values, 24×10^{-8}/year, in Çınarcık Basin, while the lowest values, 11×10^{-8}/year, are observed in Central Marmara. The highest strain rates in both edges of the fault segment in Çınarcık Basin can be indicative of a steadily creeping fault segment. In turn, lower strain rates in the Central Marmara region suggest that this segment of the NAF is locked.

Key words: Marmara Sea, North Anatolian Fault, focal mechanism, global positioning system, ocean bottom seismographs, strain rate, contraction, extension

1. Introduction

The North Anatolian Fault (NAF) extends from Karlıova triple junction to the Aegean Sea for about 1500 km (Sengör et al., 2005). It extends from Karlıova to Mudurnu Valley as a narrow fault trace. Then it enters the Marmara region where it splits into branches (Figure 1). The northern branch crosses the Gulf of İzmit, Çınarcık Basin and follows the northern shelf of the Sea of Marmara and continues from Gulf of Saros toward the Aegean and mainland Greece (Barka, 1992; Görür et al., 1997; Tüysüz et al., 1998; Okay et al., 1999; Yaltırak et al., 2000). The southern branch extends from the Mudurnu Valley towards İznik, Gemlik Bay, goes along the southern coast of the Sea of Marmara, passes east of the Marmara island, and then merges with the northern branch offshore Mürefte. Around İznik Lake, the NAF splits again into another branch that goes EW towards Bursa, Manyas, Yenice-Gönen, and then continues south-westwards Çınarcık to the Gulf of Edremit, and then again splits into branches extending in a SW direction in the Aegean Sea. Although the major earthquakes taking place along the NAF show predominantly strike-slip faulting, several moderate size earthquakes reveal normal faulting and reverse faulting mechanisms associated with transtensional and transpressional features developed along the NAF. Noticeable examples of normal faulting are the 1935 Marmara Island (Mw = 6.4), the 1964 Karacabey-Manyas (Mw = 6.9) and the 1963 Çınarcık earthquakes (Mw = 6.3). Earthquakes on transpressional features are 1983 Biga (Mw = 6.1), and the 2019 Offshore Silivri earthquake (Mw = 5.7) (Figure 1).

The NAF in the Marmara Sea between the 1999 Kocaeli earthquake rupture that extended 150 km east from central Izmit Bay, and the 1912 Ganos earthquake west of the Sea appears to be a seismic gap (Schmittbuhl et al., 2015). The Marmara Sea region is a highly populated and fast developing region of Turkey. Especially, the city of İstanbul with more than 15 million people, economic activities, Turkish industry, and its historical and cultural heritage

* Correspondence: zeynep.coskun@boun.edu.tr

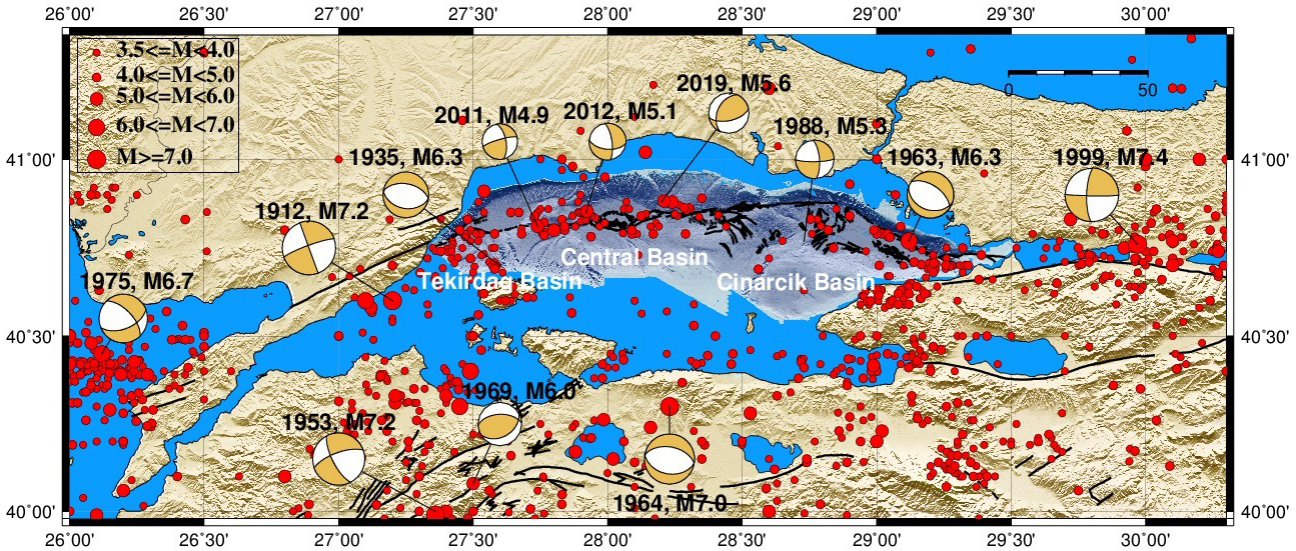

Figure 1. Seismic activity (M ≥ 3.5) in northwestern Turkey during 1900–2019 observed by Boğaziçi University Kandilli Observatory and Earthquake Research Institute Regional Earthquake-Tsunami Monitoring Center (KOERI-RETMC). Symbol sizes are proportional to magnitudes. The focal mechanisms of large historical events are illustrated as well (Map modified from Pinar et al., 2016) (Focal mechanism of large events from Vannucci and Gasperini, 2003).

faces a devastating earthquake threat. According to historical data, in the period between A.D. 1500 and 1900, six M > 7 earthquakes in 1509, 1719, 1754, May 1766 and August 1766 have occurred within the Sea of Marmara (Ambraseys and Finkel, 1990, 1991, 1995). The reevaluation of historical data by Ambraseys and Jackson (2000) states that the northern branch of the North Anatolian Fault in the Sea of Marmara between Tekidağ and Silivri has not been ruptured since 1500. This interpretation is in contrast with the general opinion that the 1766 events are the last ones that rupture the whole Main Marmara Fault (MMF) (Hubert-Ferrari et al., 2000; Fraser et al., 2010; Meghraoui et al., 2012; Drab et al., 2015). In any case, there is at least a 100 km gap between the two ruptures (Le Pichon et al., 2003).

Many geophysical, geological, and geotechnical studies have been carried out in order to characterize the NAF in the Sea of Marmara. In order to identify the potential of future expected earthquakes in the Sea of Marmara, fault geometry, fault segmentation and seismic activity along the MMF have been studied by several Ocean Bottom Seismograph (OBS) observations (Sato et al., 2004; Tary et al., 2011; Cros and Geli, 2013; Schmittbuhl et al., 2015; Yamamoto et al., 2015; Bohnhoff et al., 2016). The duration of observation periods and the extent of observation area are key factors for interpretation of the fault geometry and seismic activity beneath the Sea of Marmara.

In this study, focal mechanisms of small NAF earthquakes have been determined and used to identify transtensional and transpressional features. As described below, the seismological data are gathered from two different data sets. Small to moderate size events are investigated using broadband stations operated by KOERI-RETMC covering the period between 2002 and 2015. The microseismic activity in the Sea of Marmara is investigated by 15 OBS seismic stations deployed by JAMSTEC covering the period between September 2014 and June 2016. Furthermore, GPS data has been processed to determine the style of faulting and strain rates. The geodetic data is compiled from 112 GPS stations located around the Marmara region. The observation period extends from 1994 to 2013.

2. Data and methods

2.1. Seismic data and determination of focal mechanisms

Focal mechanisms of small to moderate size NAF earthquakes are determined from two different data sets recorded by onshore broadband stations and Ocean Bottom Seismographs (OBS). The former is obtained from broadband stations operated by Boğaziçi University Kandilli Observatory and the Earthquake Research Institute Regional Earthquake-Tsunami Monitoring Center (KOERI-RETMC) covering the period between 2002 and 2015. The latter is obtained from 15 free-fall pop-up OBS stations deployed by the Japan Agency for Marine-Earth Science and Technology (JAMSTEC) along the northern branch of the North Anatolian Fault (NAF) crossing the Marmara Sea covering the period between September 2015 and June 2016.

Focal mechanisms of events recorded by onshore seismic stations are determined using the Centroid

Moment Tensor (CMT) inversion technique developed by Kuge (2003), where the mechanisms are retrieved individually. The preprocessing of the data is carefully done before performing moment tensor inversion analysis. The success and reliability of moment tensor inversion solutions depend on the quality of the seismic records. For this purpose, seismograms are monitored using zSacWin data processing software developed by Mehmet Yılmazer, KOERI- RETMC in order to detect signals which are clipped, have gaps, spikes removed from the database. Moreover, seismograms which have good signal to noise ratios and azimuthal coverage are chosen for inversion analysis. In general, the data were bandpass filtered between 0.06 and 0.1 Hz. For smaller events (M < 3.5) higher frequencies are also used. Although several crustal structure velocity models exist for the Marmara region, the model of Kalafat et al. (1987) is used, since the observed P and S travel times fit better when compared to other models. The CMT analysis covers 99 source mechanism solutions of earthquakes with magnitudes ranging from M2.7 to M6.8 that occurred in the Sea of Marmara and surroundings, between 2002 and 2015. The locations of the events and the broadband stations are shown in Figure 2.

For the events recorded by OBSs, the method developed by Horiuchi et al. (1995) is used, where the P-wave polarity data are used. The first arrivals of P and S waves with first motion polarities of P waves are manually picked on unfiltered records. The P wave polarities of first arrivals are carefully done before performing focal mechanism analysis. The success and reliability of fault plane solutions depend on the quality of the seismic records. Since the phase readings are carried out on unfiltered data, seismograms which have good signal to noise ratio are selected for focal mechanism analysis. Focal mechanism solutions of individual small magnitude earthquakes, determined by using small number of P-wave polarity data, generally result in estimation error. In this study, after determination of first motion polarity data, the data is elaborated using the Horiuchi et al. (1995) analysis routine, where simultaneous inversion of the polarities of a cluster of earthquakes that occur in a certain small area is performed to obtain a stress tensor and focal mechanism of the individual events in the cluster. OBS analysis covers 102 source mechanism solutions of earthquakes with magnitudes ranging from M1.9 to M4.6 that occurred in the Sea of Marmara. Seventy-six out of 102 events were recorded by 10 or more OBS stations, 6 out of 102 events are recorded by less than 10 OBS stations. In order to increase the number of polarities, land seismic station records were integrated with the OBSs. The locations of the events and the broadband stations are shown in Figure 3.

2.2. GPS data and estimation of geodetic strain rates

The horizontal crustal strain rates over the Marmara Sea region are estimated using the GPS data compiled from Ergintav et al. (2014). The distribution of the compiled data of 112 GPS stations is shown in Figure 4. The station list, including the north and east component of the GPS vectors along with their standard deviations is given as a supplement file in Ergintav et al. (2014). The strain rate is estimated using the GPS data reduced to the Eurasia fixed reference frames.

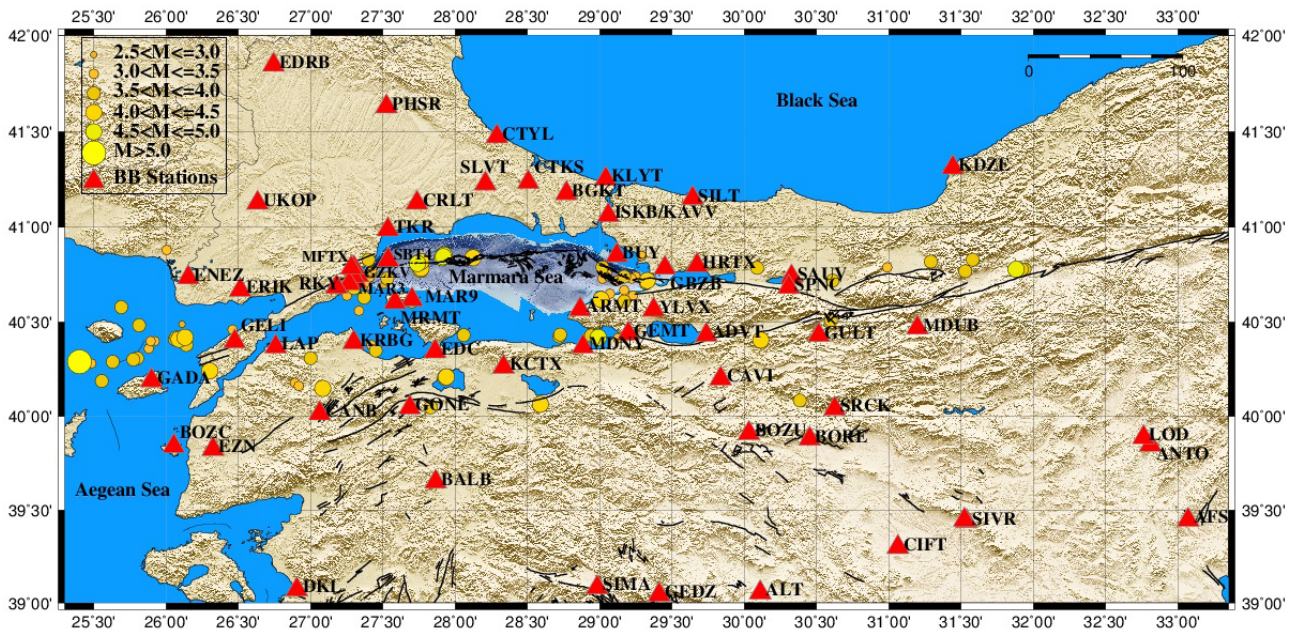

Figure 2. Locations of events and the broadband stations selected for CMT analysis. Symbol sizes of earthquakes (yellow circles) are proportional to magnitude. Red triangles indicate broadband seismic stations.

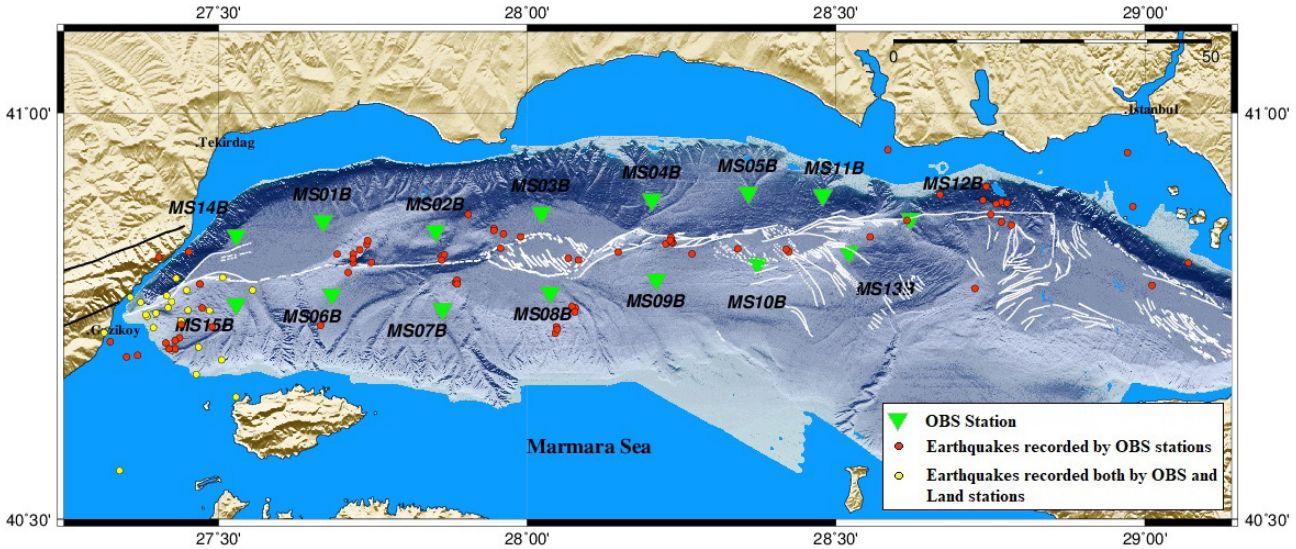

Figure 3. Locations of events with magnitude between 1.9 and 4.6 recorded by OBS and land seismic stations between 2013 and 2016. Green triangles indicate the location of OBS stations. Yellow circles indicate events recorded by OBS and land seismic stations. Red circles indicate events recorded by only OBS stations.

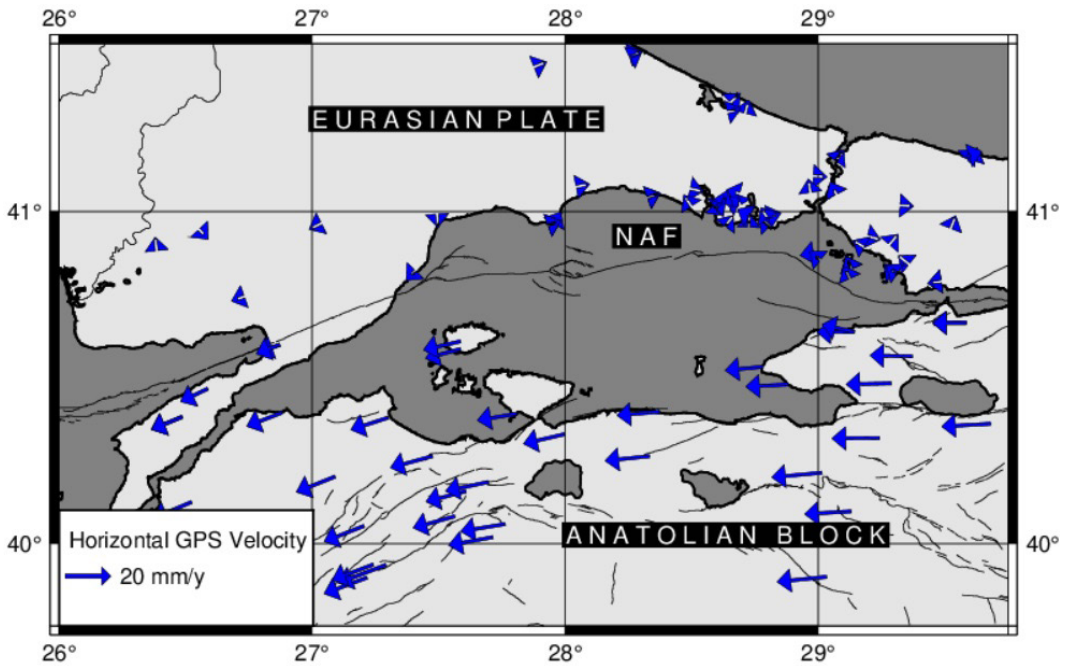

Figure 4. The blue-colored arrows denote the GPS horizontal velocities with respect to Eurasian Plate given in Ergintav et al. (2014). The time span of GPS observation is about 20 years. The solid black lines are the active faults in the Marmara region. NAF (North Anatolian Fault) is the boundary between Eurasian Plate and Anatolian Block.

The observation period varies from station to station from 1994 to 2013. The computed horizontal velocities with a precision less than 1 mm/year are between 1 and 24 mm/year. Note that the stations located on the northern block of NAF are located on the Eurasian plate used as a reference frame. As such, the GPS data are similar to the estimates obtained by others (Meade et al., 2002; Reilinger et al., 2006; Hergert et al., 2011).

Several studies show how horizontal GPS velocities can be used to determine the strain rate tensors (e.g., Hackl et al., 2009; Kreemer et al., 2014a; Kreemer et al., 2014b; Ashurkov et al., 2016). The gradients of the velocities are

calculated along the northern and eastern directions that give continuous strain fields with values corresponding to strain rate tensor components estimated as:

$$\dot{\varepsilon}_{ee} = \frac{\delta \upsilon_e}{\delta x_e} \quad (1)$$

$$\dot{\varepsilon}_{nn} = \frac{\delta \upsilon_n}{\delta x_n} \quad (2)$$

$$\dot{\varepsilon}_{en} = \frac{1}{2}\left(\frac{\delta \upsilon_e}{\delta x_e} + \frac{\delta \upsilon_n}{\delta x_n}\right) \quad (3)$$

where u is the GPS velocity at the point x; *e* is the longitude, and *n* is the latitude. Having estimated the strain tensor components at each grid point, the direction (a_1, a_2) and magnitude ($\dot{\varepsilon}_1$, $\dot{\varepsilon}_2$) of the principal strains is calculated as:

$$\tan 2\alpha_1 = \frac{2\dot{\varepsilon}_{en}}{\dot{\varepsilon}_{nn} - \dot{\varepsilon}_{ee}} \quad (4)$$

$$\tan 2\,\alpha_2 = \frac{2\dot{\varepsilon}_{en}}{\dot{\varepsilon}_{nn} - \dot{\varepsilon}_{ee}} \pm 90° \quad (5)$$

$$\dot{\varepsilon}_{1,2} = \frac{1}{2}\left(\dot{\varepsilon}_{ee} + \dot{\varepsilon}_{nn}\right) \pm \sqrt{\left(\dot{\varepsilon}_{ee} - \dot{\varepsilon}_{nn}\right) + 4\dot{\varepsilon}_{en}^2}$$

where $\dot{\varepsilon}_1 > 0$, $\dot{\varepsilon}_1 > \dot{\varepsilon}_2$ (6)

The sum of the diagonal elements of the tensor gives the rate of relative change of area (volume change) and provides the possibility to identify regions of contraction or extension (Hackl et al., 2009). The dilatation rate (δ) is estimated as:

$$\delta = \dot{\varepsilon}_1 + \dot{\varepsilon}_2 \quad (7)$$

The directions of maximum shear strain help define the likely directions of the strike-slip faults (dextral and sinistral). The maximum shear strain rate γ_{max} and its directions $\theta_{1,2}$ are found as:

$$\gamma_m = (\dot{\varepsilon}_1 - \dot{\varepsilon}_2) \quad (8)$$

and

$$\tan 2\theta_1 = \frac{\dot{\varepsilon}_{nn} - \dot{\varepsilon}_{ee}}{2\dot{\varepsilon}_{en}} \quad (9)$$

$$\tan 2\,\theta_2 = \frac{\dot{\varepsilon}_{nn} - \dot{\varepsilon}_{ee}}{2\dot{\varepsilon}_{en}} \pm 90° \quad (10)$$

The style of strain rate tensor, S, is determined as:

$$S = (\dot{\varepsilon}_1 + \dot{\varepsilon}_2)/max\,(|\dot{\varepsilon}_1|, |\dot{\varepsilon}_2|) \quad (11)$$

S can be used to approximately quantify the type of displacement into extension (S > 0.5), strike-slip (0.5 < S < −0.5), and contraction (*S* < −0.5). The second invariant of the strain rate tensor (I_2) is estimated as:

$$I_2 = \sqrt{\dot{\varepsilon}_{ee}^{\,2} + \dot{\varepsilon}_{nn}^{\,2} + 2\dot{\varepsilon}_{en}^{\,2}} \quad (12)$$

3. Results

3.1. Focal mechanism results

3.1.1. CMT Results

Multiple solutions, giving a range of possible moment magnitude values, depth values, and focal mechanisms, are obtained for each earthquake. The best solution for each earthquake is chosen using variance reduction. The earthquakes in the dataset are relocated and their fault plane solution is retrieved using the CMT technique developed by Kuge (2003). The solutions obtained by inversion are then examined in terms of variance reduction and fault plane variations versus source depth and unreliable solutions are eliminated from generated CMT catalogue. The reliability of the solutions is also based on the variation of produced focal mechanisms for each event. The solution is accepted as sufficiently accurate when a clear best focal mechanism and other produced solutions show similar focal mechanisms. On the other hand, when small changes in the source depth lead to very different mechanisms, the solution is considered inaccurate.

The CMT inversion is mainly carried out using broadband records and the results are given in Supplementary Table 1 and Figure 5. For the case of May 24th, 2014 Mw 6.8 Gökçeada earthquake, where the near-source broadband seismometers are clipped, the moment tensor inversion is carried out using acceleration data.

Ganos Area

The first remarkable finding of this study is related to the segmentation and bending between the Ganos Fault and Tekirdag Basin (Figure 6). In the west, between the Ganos Fault and the Tekirdag Basin, along with the strike-slip faulting mechanism, the CMT inversion results show significant number of events having reverse faulting mechanism with NW trending compressional stress, which is consistent with the fault plane solution of the 27 April 1985 Mürefte earthquake (M = 4.4) located in the Ganos Mountain.

Eastern Marmara Segment

Another remarkable seismotectonic feature is observed in eastern Marmara region inferred from the focal mechanisms in the Yalova-Çınarcık and Çınarcık basin locations. Despite the proximity of the two locations, the focal mechanisms in the Yalova-Çınarcık region show predominantly N-S extension while the Çınarcık basin events show NE-SW extension (Figure 7). That is to say the stress fields to the north of NAF and the stress field to the south of NAF is rotated by about 45 degrees. The results are also consistent with the stress tensor inversion study of Pinar et al. (2003), Bulut et al. (2009), and Pinar et al. (2016). Moreover, various types of focal mechanisms are observed in the Çınarcık Basin, as strike-slip, normal faulting and reverse faulting mechanism may result from the presence of a segmented fault system where restraining local stresses are developed.

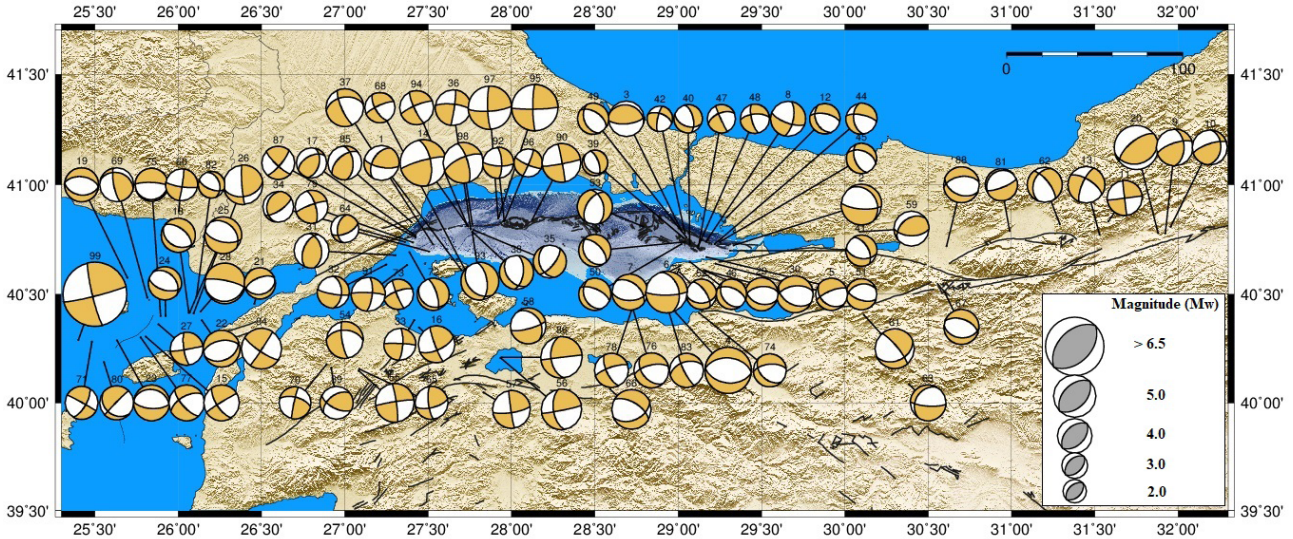

Figure 5. The location of earthquakes and moment tensor inversion results of the events around Marmara region. Symbol sizes are proportional to magnitude. The events and their source parameters are given in Supplementary Table 1.

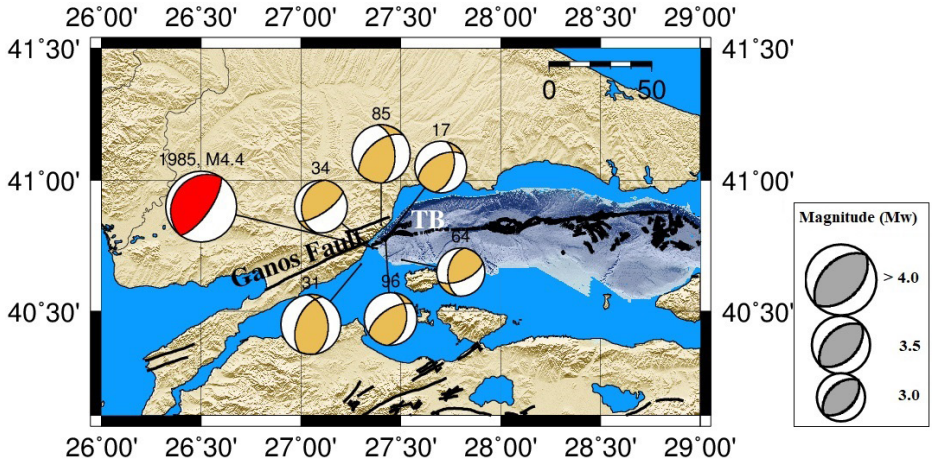

Figure 6. CMT inversion results having reverse faulting mechanism between the Ganos Fault and Tekirdag Basin. The solution of 1985 Mürefte Earthquake by Kalafat (1995) is given in red. Symbol sizes are proportional to magnitudes, TB: Tekirdag Basin. The events and their source parameters are given in Supplementary Table 1.

NAF near Bolu City

The detection of three earthquakes having pure reverse and reverse with minor strike-slip component faulting mechanisms that occurred 4 km away from the major dextral NAFZ near Bolu City is another unexpected finding of this study. The existence of the NAF as the one and only active major fault in the region (beside local faults) suggests us that tectonic activity along the NAF and the Pontides are related to each other. The ongoing tectonism and seismicity along the NAF may result in stress accumulation along the surrounding zones forced by the shearing on NAF, and thus triggering the tectonic evolution of thrusts and strike slip faulting in the northern region of main NAF. Both the focal mechanisms of the reverse and reverse with minor strike-slip faulting types show maximum compressional directions oriented NW-SE. This stress regime is consistent also with the focal mechanism of the 1968 Bartin earthquake (Mw = 6.5) which is strong evidence for the relation between the driving forces of the tectonics along NAF and Pontides (Figure 8).

3.1.2. Simultaneous inversion of first motion polarity data results

The analysis of microearthquakes recorded by OBS stations deployed closely around the NAF in the Sea of

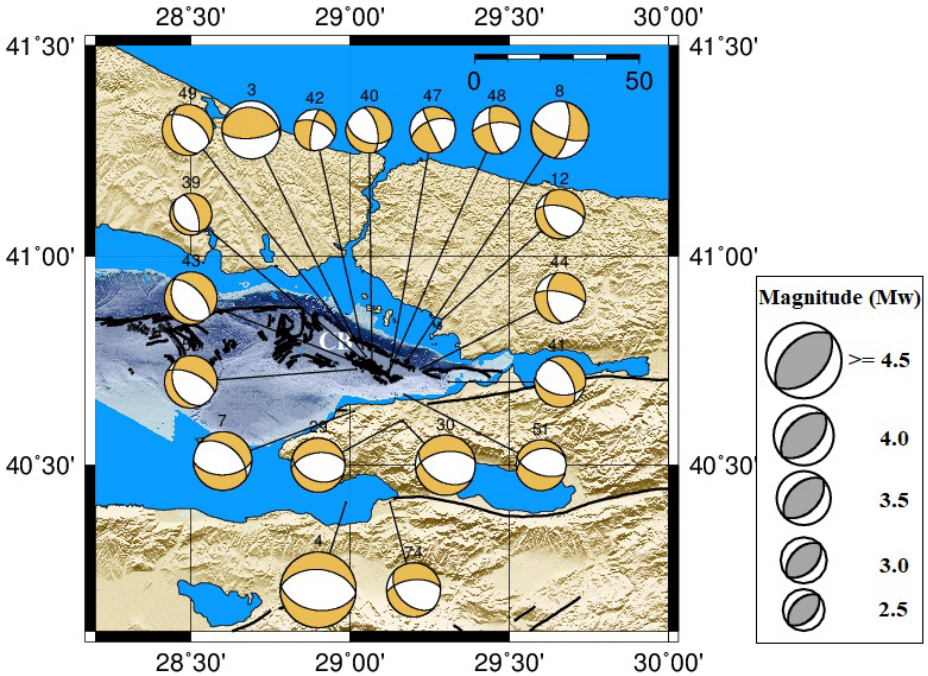

Figure 7. CMT inversion results in the Çınarcık Basin. Symbol sizes are proportional to magnitudes, CB: Çınarcık Basin. The events and their source parameters are given in Supplementary Table 1.

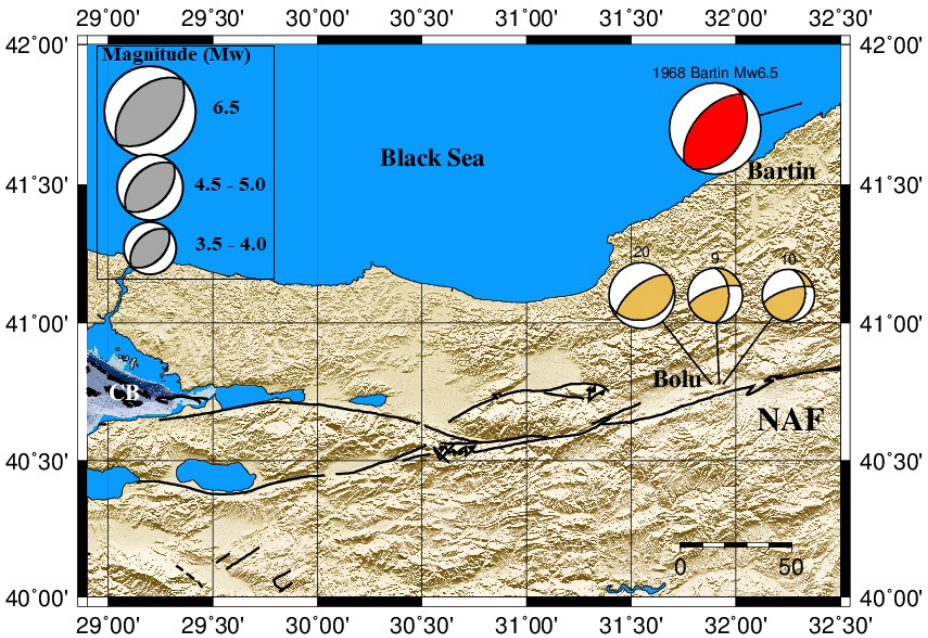

Figure 8. CMT inversion results of three earthquakes having pure reverse and reverse with minor strike-slip component faulting mechanisms in Bolu Province. Symbol sizes are proportional to magnitudes. NAF: North Anatolian Fault. The events and their source parameters are given in Supplementary Table 1.

Marmara provides considerable information about the seismic activity and the seismogenic zone along different segments of the MMF.

Ganos Area

The data acquired in the Ganos area include 37 events with magnitudes between 2.0 and 4.1. For this cluster,

a total of 645 P-wave polarities are used to determine focal mechanisms. The focal mechanism results and source parameters are given in Supplementary Table 2 and Figure 9.

Between the Ganos Fault and Tekirdag Basin, along with the strike-slip and normal faulting mechanisms, the results show a significant number of events having reverse faulting mechanism with NW trending compressional stress which are consistent with the results obtained from CMT analysis. The hypocenter locations of the events that occurred in the Ganos area change between about 5 km and 19 km depth (Figure 9).

Western Marmara Segment

The data acquired in the Western Marmara Segment include 38 events with magnitudes between 1.8 and 4.6. For this cluster, a total of 434 P-wave polarities are used to determine focal mechanisms. The focal mechanism results and source parameters are given in Supplementary Table 3 and Figure 10. The focal mechanisms determined along Western Marmara segment show mostly strike-slip and normal faulting style. There are also several events that exhibits thrust faulting around Central Basin.

Central Marmara Segment

The data acquired in Central Marmara Segment include 24 events with magnitudes between 1.9 and 4.2. For this cluster, a total of 273 P-wave polarities are used in order to determine focal mechanisms. The focal mechanism results and source parameters are given in Supplementary Table 4 and Figure 11. Although ten M > 3.0 earthquakes occurred in this cluster, the seismic activity is visibly less than for the Ganos and Western Marmara segments. Moreover, results indicate that there is no seismicity along with Main Marmara Fault between the Kumburgaz Basin and the western Çınarcık Basin.

The results further indicate that the Tekirdag Basin, Western High, and Central Basin are the most seismically active part in Marmara Sea when compared to the eastern segments. The deepest events up to 20–24 km are also observed along the Western Marmara Segment, namely the Western High and Central Basin. To the west, in the Ganos Area, the depths of the events observed are in the range of 5–19 km. When it comes to the Central Marmara Segment, between the eastern Central Basin and western Çınarcık Basin, the seismic activity is reduced compared to the western segments. Besides, the eastern segments accommodate shallower seismicity. The events generally occur at 7 km deep; the deepest event observed in this region is ≈ 12 km.

In the entire data set, covering microearthquakes and small to moderate size events, the results indicate that there

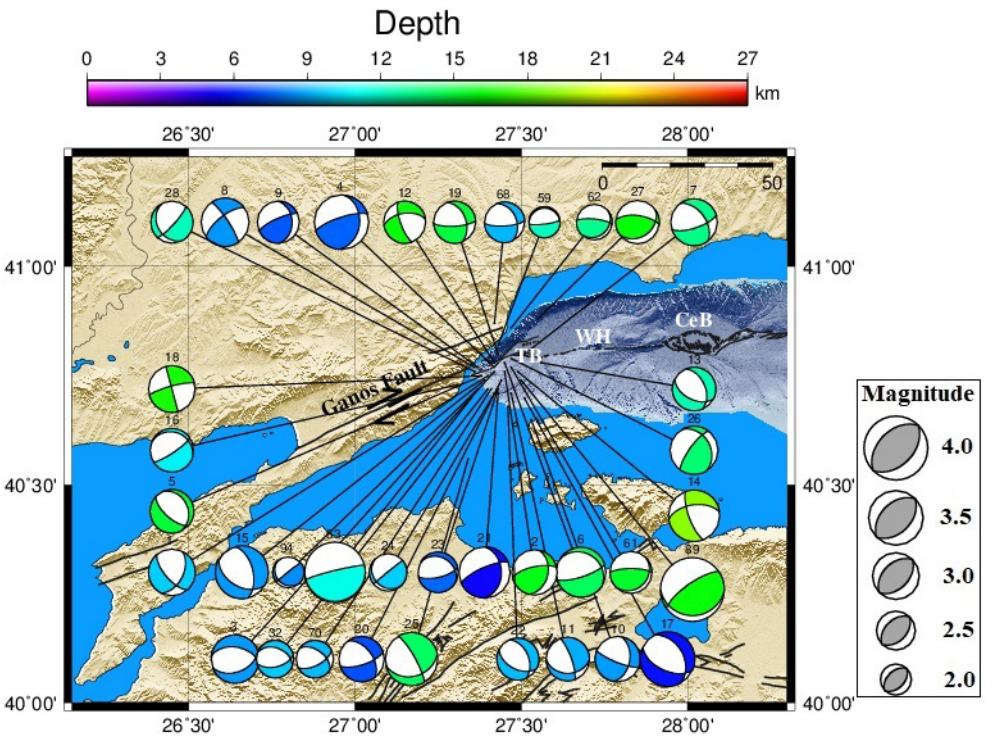

Figure 9. Focal mechanisms derived from simultaneous inversion of the polarity data acquired in Ganos Area. Symbol sizes are proportional to magnitudes. The color and size of beach ball denote depth and moment magnitude, respectively. The events and their source parameters are given in Supplementary Table 2.

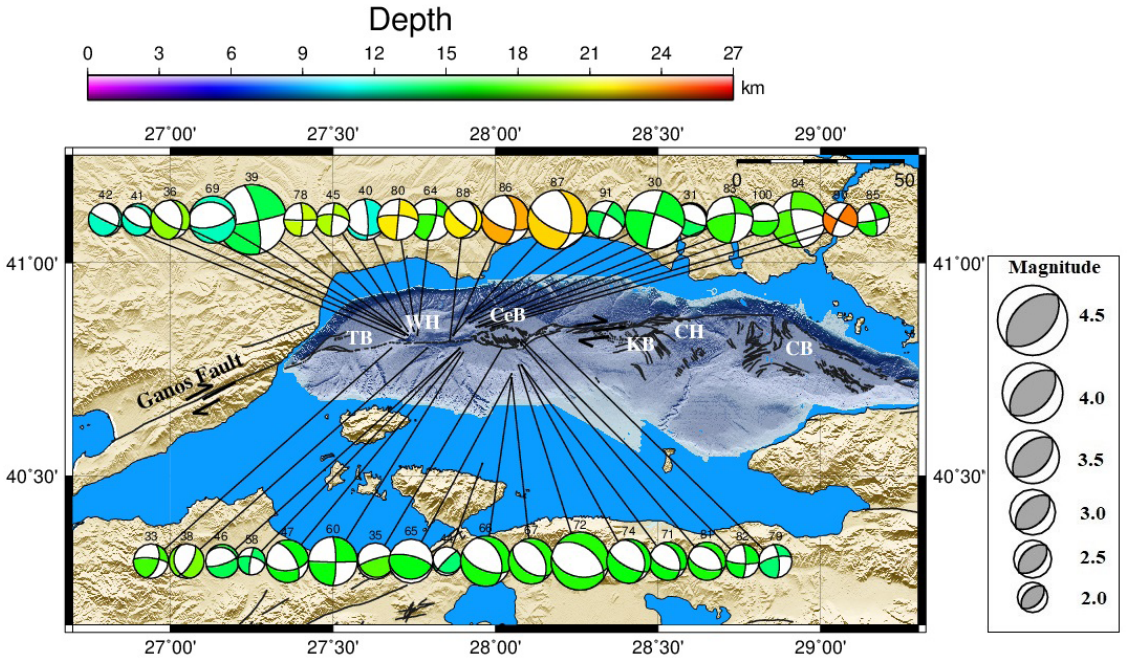

Figure 10. Focal mechanisms derived from simultaneous inversion of the polarity data acquired in Western Marmara Segment. KB: Kumburgaz Basin, CH: Central High, CB: Çınarcık Basin. Symbol sizes are proportional to magnitudes. The color and size of beach ball denote depth and moment magnitude, respectively. The events and their source parameters are given in Supplementary Table 3.

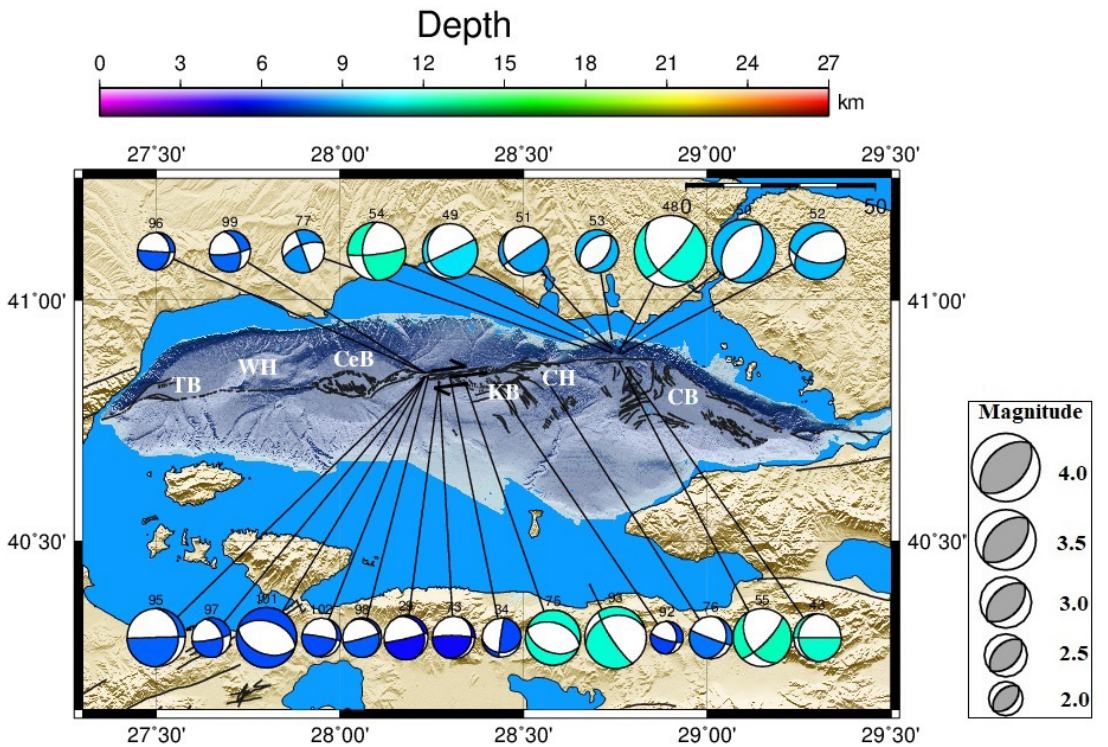

Figure 11. Focal mechanism derived from simultaneous inversion of the polarity data acquired in Central Marmara Segment. Symbol sizes are proportional to magnitudes. The color and size of beach ball denote depth and moment magnitude, respectively. The events and their source parameters are given in Supplementary Table 4.

is almost no seismic activity in the Kumburgaz Basin. The results are also consistent with the latest studies of Lange et al. (2019) and Schmitbuhl et al. (2015) indicating the low seismicity in the Kumburgaz Basin along the MMF. The sparse seismicity beneath the Kumburgaz Basin, bounded by high levels of seismicity on both edges, suggests that this section of the NAF is locked and so accumulating strain (Lange et al, 2019; Schmitbuhl et al, 2015; Yamamoto et al, 2015).

3.2. Geodetic strain rates

Distance and areal weighting functions are applied to derive the smoothly interpolated continuous strain field maps. Gaussian and Quadratic functions are applied for distance weighting. On the other hand, Voronoi cell and azimuthal functions are applied for areal weighting that evaluates the density of the GPS observations. An optimal interpolation model has been determined through examination of differential strain-rate patterns of two strain-rate fields derived using different net weighting threshold, Wt, in a way described by Shen et al. (2015). Wt = 10 has been selected as an optimal smoothing model for this study. According to the GPS strain rate results, the highest values, approximately 24×10^{-8}/year, are observed in the Çınarcık Basin, while the lowest values, 11×10^{-8}/year, are observed in the Central Marmara (Figure 12).

The strain rate tensor style S can be used to determine the type of tectonic regime prevailing in a region. The predominant contractional regions correspond to areas where $S < -0.5$, the strike-slip regime is characterized by $0.5 < S < -0.5$, and extension is represented by $S > 0.5$. The spatial variations in the style of strain rate tensor are shown in Figure 13, where distinct tectonic features can be easily noticed. Extensional and strike-slip style dominate Marmara region, while compressional features are rare.

The dilation strain rates of positive and negative regions in the Marmara Sea region are depicted, suggesting that elongation and contraction of the crust coexist (Figure 14). Significant elongation is observed in the Çınarcık Basin and the area between Marmara Island and the Central Basin. Moreover, the dilatation map depicts elongations in the area to the north of Saros Bay.

The maximum and minimum principal strain axes identify the direction of extension and contraction. The minimum horizontal principal strain axes are oriented NE-SW, but the maximum strain axes are oriented NW-SE in almost the entire Marmara Sea. Such features have also been derived from the stress tensor inversion of the focal mechanisms.

Contractional or transpressional features are also inferred for some locations in Marmara region (Figure

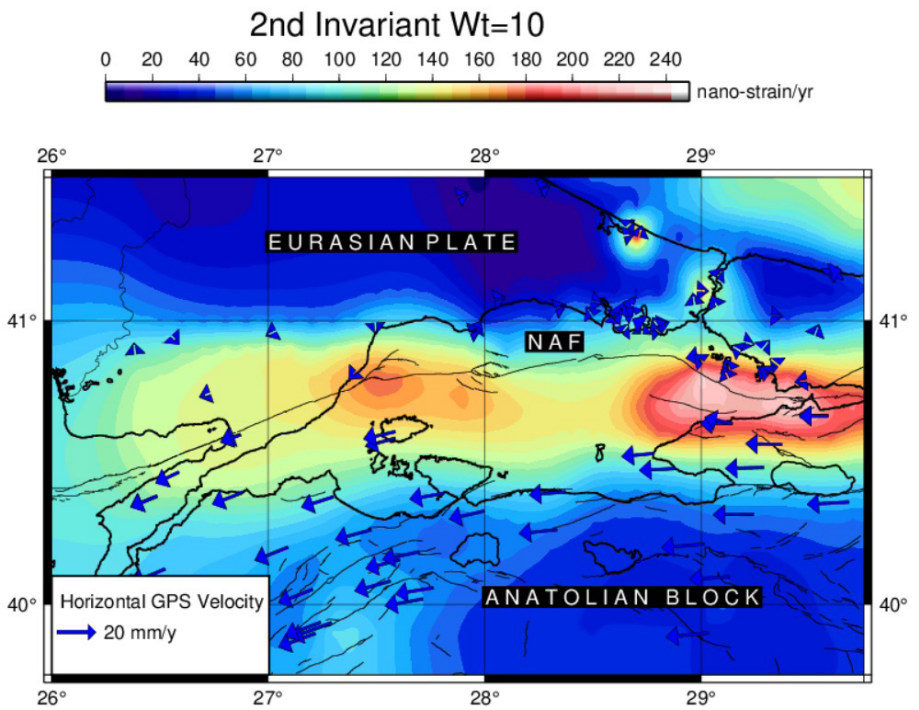

Figure 12. The second invariant of strain Rates (background) using Gaussian and Voronoi cell weighting functions with net weighting thresholds set as Wt = 10. The blue-colored arrows denote the GPS horizontal velocities with respect to Eurasian Plate given in Ergintav et al. (2014). The solid black lines are the active faults in Marmara region. NAF (North Anatolian Fault) is the boundary between Eurasian Plate and Anatolian Block.

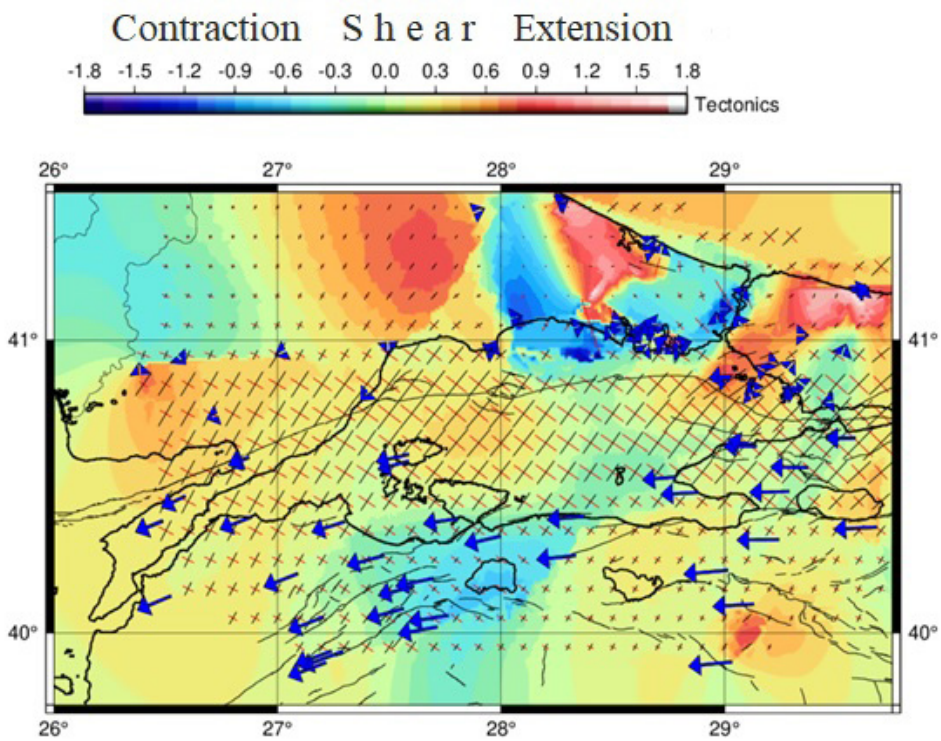

Figure 13. The strain rate tensor style S is used to determine the type of tectonic regime prevailing in the region. The predominant compressional regions correspond to areas where $S < -0.6$, the strike-slip regime is characterized by $0.6 < S < -0.6$, and extension is represented by $S > 0.6$. The size and orientation of the minimum and maximum principal strain rate axis are shown with black and red lines, respectively.

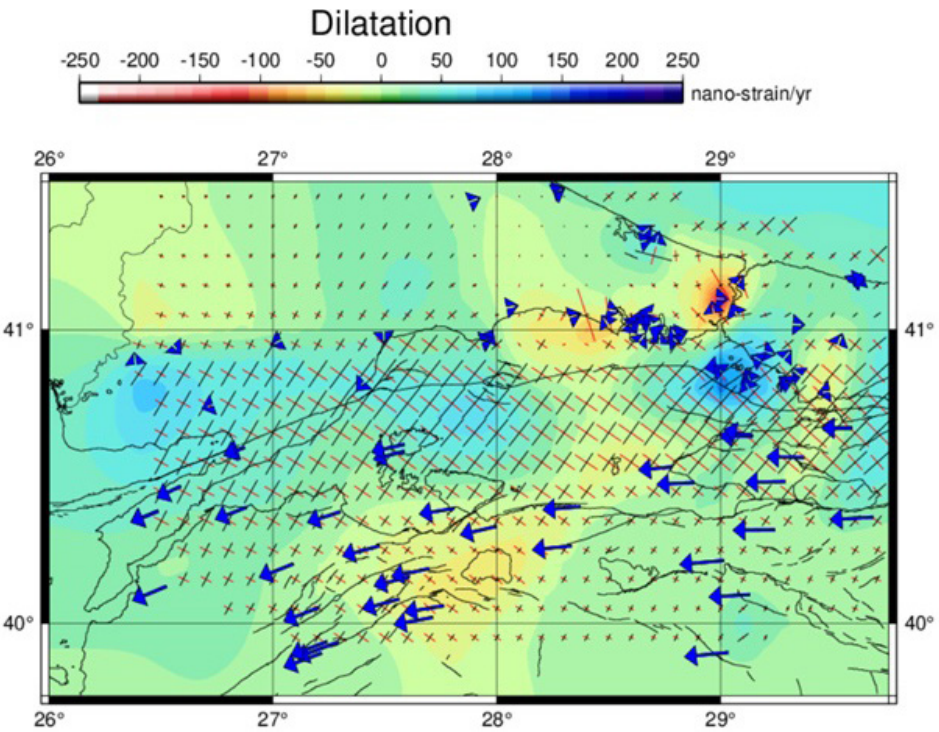

Figure 14. Dilatation strain rate map (background). Positive dilatation corresponds to extension and negative to contraction. The orientations of the minimum and maximum principal strain rate axis are shown with black and red lines, respectively.

14). The Central segment extending from the Central Basin eastward toward the Çınarcık Basin is an example of such a contractional area. We note that the 26 September 2019 event of Mw = 5.7 took place in the area to the east of the Central Basin showing predominantly an oblique reverse faulting mechanisms. Similarly, the area to the west of Marmara Island and Ganos also points out contraction where several reverse faulting mechanisms have been obtained from the seismological data.

4. Discussion and conclusion

The contractional and extensional features together with the seismic activity beneath the Sea of Marmara and surroundings are examined using both seismological and geodetic data.

The first important finding is related to the segmentation and bending between the Ganos Fault and the Tekirdag Basin. The transpression in this area is reflected in the morphology, forming the Ganos Mountain, a major zone of uplift, 10 km wide and 35 km long, elongated parallel to the transpressional Ganos Fault segment west of this bend (Okay et al., 2000). To the west, between the Ganos Fault and Tekirdag Basin, along with the strike-slip faulting mechanisms, the focal mechanism solutions of microearthquakes derived by the simultaneous inversion of first motion polarity data by OBS and land seismic stations show a significant number of events having reverse faulting mechanism with NW trending compressional stress. We note that these results are consistent with the fault plane solutions of small to moderate size events determined by CMT analysis and also fault plane solution of the M4.4 27 April 1985 Mürefte earthquake located in the Ganos Mountain, which gives a reverse fault mechanism with a NE striking fault plane.

As a result of detailed analysis, a considerable number of varying types of focal mechanisms are observed which reveal the presence of a segmented fault system where restraining local stresses are developed. Our results show that the Tekirdag Basin, Western High, and Central Basin are the most seismically active parts in Marmara Sea when compared to eastern segments. The deepest events, up to 20–24 km deep, are also observed in Western High and Central Basin. The sparse seismicity beneath the Kumburgaz Basin, in spite of the high level of seismicity on both edges suggests that this section of the NAF is locked and so accumulating strain.

In the spatial variations in the style of the strain rate tensor, distinct tectonic features can be noticed. Extensional and strike-slip styles dominate the Marmara region, while contractional features are rare. Such features are also derived from the focal mechanism solutions obtained using seismological data. Significant elongation is observed in the Çınarcık Basin and the area between Marmara Island and the Central Basin. Moreover, the dilatation map depicts extension in the area to the north of Saros Bay. The Central segment extending eastward from the Central Basin toward the Çınarcık Basin is an example of such a contractional area. We note that the 26 September 2019 event of Mw = 5.7 took place in the area to the east of the Central Basin showing predominantly an oblique reverse faulting mechanism. Similarly, the area to the west of Marmara island and Ganos also point out contraction where several reverse faulting mechanisms have been obtained from the seismological data.

According to the GPS shear strain rate results, the highest values, 24×10^{-8}/year, are observed in Çınarcık Basin, while the lowest values, 11×10^{-8}/year, are observed in Central Marmara. These results are retrieved using an optimal smoothing model described in Section 3.2. The strain-rate values are quite dependent on choice of regularization used in the strain-field determination.

This is quite evident from the comparison of the 2nd invariant strain-rate map and the trace of the NAF in the Çınarcık Basin. The Çınarcık Basin segment of the NAF bisects the ENW-ESE extending a large strain-rate area where the southern part represents the Anatolian Block and the northern parts represent the Eurasian Plate. This result portrays freely sliding along the Çınarcık Basin segment (Figure 12). Pinar et al. (2016) utilized the focal mechanisms of several Çınarcık Basin earthquakes and the regional stress field acting in the Eastern Marmara region and suggested that the fault segment crossing the Çınarcık Basin is a weak fault. They compared the azimuths of the P- and T-axes of the focal mechanisms with the orientation of the maximum and minimum principal compressive stress, respectively, and found out that the P-axis azimuths are aligned with the direction of the maximum compressive stress axis and the T-axis azimuths are in-line with the azimuth of the minimum compressive stress axis based on the methodology given in Iio (1996).

On the contrary, the NAF fault segment and the 2nd invariant strain-rate field between Central Basin and Çınarcık Basin depict a quite different picture (Figure 12). Here, the fault trace outlines a border between high and low strain-rate places implying a locked fault trace between the Anatolian Block and the Eurasian Plate. There are three main fault segments (eastern, central, and western) crossing the Sea of Marmara to be ruptured by the next major earthquake. The 2nd invariant map suggests that the central segment is locked and the eastern segment is freely sliding. As per the 2nd invariant map in Figure 12, parts of the western segment also depicts a picture similar to the eastern segment. A long-term of 3.5–year observations carried out using five sea bottom extensometers deployed on the fault trace crossing the western high show a creeping rate of around 11 mm/year in that region (Yamamoto et al., 2019). Moreover, it is obvious from Figure 12 that the southern Marmara strand

of the NAF represents a border between high- and low strain-rate sites. Okay et al. (2000) define the boundary region of low and high strain-rate sites as the Southern Branch of NAF where the GPS results point out strain accumulation along that branch of NAF is taking place.

Acknowledgments
The waveform data used for CMT inversion were obtained from KOERI-RETMC seismic network. All the figures were created using Generic Mapping Tools (Wessel and Smith, 1991). OBS observations were conducted under the Marmara Disaster Mitigation (MarDIM) project, formally known as the Earthquake and Tsunami Disaster Mitigation in the Marmara Region and Disaster Education in Turkey project. MarDIM receives financial support from the Japan International Cooperation Agency, Japan Science and Technology Agency, and the Ministry of Development in Turkey.

References

Ambraseys NN, Finkel CF (1990). The Marmara Sea Earthquake of 1509. Terra Nova 2: 167-174.

Ambraseys NN, Finkel CF (1991). Long-term seismicity of Istanbul and the Marmara Sea region. Terra Nova 3: 527-539.

Ambraseys NN, Finkel CF (1995). The Seismicity of Turkey and Adjacent Areas, a Historical Review, 1500-1800. Eren Yayıncılık, İstanbul.

Ambraseys NN, Jackson JA (2000). Seismicity of the Sea of Marmara (Turkey) since 1509. Geophysical Journal International 141: F1-F6.

Ashurkov SV, San'Kov VA, Serov MA, Luk'Yanov PY, Grib NN et al. (2016). Evaluation of present-day deformations in the Amurian Plate and its surroundings, based on GPS data. Russian Geology and Geophysics 57: 1626–1634.

Barka AA (1992). The North Anatolian fault zone. Annales Tectonicae, Special Issue, VI: 164–195.

Bulut F, Bohnhoff M, Ellsworth W, Aktar M, Dresen G (2009). Microseismicity at the North Anatolian fault in the Sea of Marmara offshore Istanbul, NW Turkey. Journal of Geophysical Research http://doi.org/10.1029/2008JB00624.

Cros E, Géli L (2013). Characterisation of microseismicity in the Western Sea of Marmara: Implications in terms of seismic monitoring http://doi.org/10.13155/38916.

Ergintav S, R. E. Reilinger, R. Çakmak, M. Floyd, Z. Cakir et al. (2014). Istanbul's earthquake hot spots: Geodetic constraints on strain accumulation along faults in the Marmara seismic gap. Geophysical Research Letters 41: 5783–5788, https://doi.org/10.1002/2014GL060985

Hergert T, Heidbach O, Becel A, Laigle M (2011). Geomechanical model of the Marmara Sea region -1. 3-D contemporary kinematics. Geophysical Journal International 185: 1073–1089.

Horiuchi S, Rocco G, Hasegawa A (1995). Discrimination of fault planes from auxiliary planes based on simultaneous determination of stress tensor and a large number of fault plane solutions. Journal of Geophysical Research 100 (5): 8327–8338.

Hubert-Ferrari A, Barka A, Jacques E, Nalbant S, Meyer B et al. (2000). Seismic hazard in the Marmara sea region following the 17 August 1999 Izmit earthquake. Nature 404: 269-273.

Iio Y (1997). Frictional coefficient on faults in a seismogenic region inferred from earthquake mechanism solutions. Journal of Geophysical Research, 102: 5403–5412.

Kalafat D (1995). Study of the tectonic structures in Anatolian based on fault mechanism 681 solutions. PhD thesis, University of Istanbul, 217 pp. (in Turkish), Istanbul, Turkey.

Kalafat D, Gürbüz C, Üçer SB (1987). Batı Türkiye'de Kabuk ve Üst Manto Yapısının Araştırılması. Deprem Araştırma Bülteni 59: 43–64 (in Turkish).

Ketin İ (1968). Relations between general tectonic features and the main earthquake regions in Turkey. Bulletin of the Mineral Research and Exploration Institute of Turkey 71: 63–67.

Kikuchi M, Kanamori H (1991). Inversion of complex body waves-III. Bulletin of the Seismological Society of America 81: 2335-2350.

Kohketsu K (1985). The extended reflectivity method for synthetic near-field seismograms. Journal of Physics of the Earth 33: 121–131.

Kostrov VV (1974). Seismic Moment and Energy of Earthquakes, and Seismic Flow of Rocks. Izvestiya Academy of Sciences of the USSR, Physics of the Solid Earth 1: 23-44.

Kreemer C, Blewitt G, Klein EC (2014). A geodetic plate motion and Global Strain Rate Model. Geochemistry, Geophysics, Geosystems 15 (10): 3849-3889.

Kuge K (2003). Source modeling using strong-motion waveforms: toward automated determination of earthquake fault planes and moment-release distributions. Bulletin of the Seismological Society of America 93: 639–654.

Kuge K, Kawakatsu H (1993). Significance of non-double couple components of deep and intermediate-depth earthquakes: implications from moment tensor inversions of long-period seismic waves. Physics of the Earth and Planetary Interiors 75: 243–266.

Kurt H, Sorlien CC, Seeber L, Steckler MS, Shillington DJ et al. (2013). Steady late quaternary slip rate on the Cinarcik section of the North Anatolian fault near Istanbul, Turkey. Geophysical Research Letters 40: 4555–4559. http://doi.org/10.1002/grl.50882

Laigle M, Bécel A, de Voog B, Hirn A, Taymaz T et al. (2008). The Members of the SEISMARMARA Leg1, A first deep seismic survey in the Sea of Marmara: whole crust and deep basins. Earth and Planetary Science Letters 270: 168–179.

Lange D, Kopp H, Royer JY, Henry P, Cakir Z et al. (2019). Interseismic strain build-up on the submarine North Anatolian fault offshore Istanbul. Nature Communications 10 (1): 9.

Lawson CL, Hanson RJ (1974). Solving Least Squares Problems, SIAM, Philadelphia.

Lee WHK, Lahr JC (1972). HYPO71: a computer program fordetermining hypocenter, magnitude and first-motion patternof local earthquakes, U.S. Geological Survey Open-File Report, pp. 100.

Le Pichon X, Taymaz T, Şengör AMC (1999). The Marmara Fault and the Future Istanbul Earthquake", Proceedings of ITU-IAHS, International Conference on the Kocaeli Earthquake 17 August 1999, İstanbul, Turkey, 1999 December 2–5, pp. 41–54.

X Le Pichon, Chamot-Rooke N, Rangin C, Sengör AMC (2003). The North Anatolian fault in the Sea of Marmara. Journal of Geophysical Research 108 (B4): 2179. http://doi.org/10.1029/2002JB001862

Meade BJ, Hager BH, McClusky SC, Reilinger RE, Ergintav S et al. (2002). Estimates of seismic potential in the Marmara region from block models of secular deformation constrained by GPS measurements. Bulletin of the Seismological Society of America 92: 208– 215.

Meghraoui M, ME Aksoy, Akyüz HS, Ferry M, Dikbaş A et al. (2012). Paleoseismology of the North Anatolian Fault at Güzelköy (Ganos segment, Turkey): Size and recurrence time of earthquake ruptures west of the Sea of Marmara. Geochemistry, Geophysics, Geosystems 13, Q04005. http://doi.org/10.1029/2011GC003960

Okay Aİ, Demirbağ E, Kurt H, Okay N, Kuşcu İ (1999). An active, deep marine strike–slip basin along the North Anatolian Fault in Turkey. Tectonics 18: 129–148.

Okay A, Kaslilar-Özcan A, Imren C, Boztepe-Güney A, Demirbag E et al. (2000). Active faults and evolving strike-slip basins in the Marmara Sea, northwest Turkey: a multichannel seismic reflection study. Tectonophysics 321: 189–218.

Pinar A, Kuge K, Honkura Y (2003). Moment tensor inversion of recent small to moderate sized earthquakes: Implications for seismic hazard and active tectonics beneath the Sea of Marmara. Geophysical Journal International 153: 133–145. http://doi.org/10.1046/j.1365-246X.2003.01897.x

Pinar A, Coşkun Z, Mert A, Kalafat D (2016). Frictional strength of North Anatolian fault in eastern Marmara region. Earth, Planets and Space 68-62, https://doi.org/10.1186/s40623-016-0435-z.

Polat A, Tatar O, Gürsoy H, Yalçiner CÇ, Büyüksaraç A (2012). Two-phased evolution of the Suşehri Basin on the North Anatolian Fault Zone, Turkey. Geodinamica Acta 25: 3-4: 132-145. http://doi.org/10.1080/09853111.2013.861997

Reilinger R, McClusky S, Vernant P, Lawrence S, Ergintav S et al. (2006). GPS constraints on continental deformation in the Africa-Arabia-Eurasia continental collision zone and implications for the dynamics of plate interactions. Journal of Geophysical Research 111: B05411. http://doi.org/10.1029/2005JB004051

Sato T, Kasahara J, Taymaz T, Ito M, Kamimura A et al. (2004). A study of microearthquake seismicity and focal mechanisms within the Sea of Marmara (NW Turkey) using ocean bottom seismometers (OBSs). Tectonophysics 391: 303–314 http://doi.org/10.1016/j.tecto.2004.07.018

Schmittbuhl J, Karabulut H, Lengliné O, Bouchon M (2015). Seismicity distribution and locking depth along the Main Marmara Fault, Turkey. Geochemistry, Geophysics, Geosystems 17: 954–965. http://doi.org/10.1002/2015GC006120

Shen Zheng-Kang, Wang M, Zeng Y, Wang F (2015). Optimal Interpolation of Spatially Discretized Geodetic Data. Bulletin of the Seismological Society of America 105 (4): 2117.

Tary JB, Geli L, Henry P, Natalin B, Gasperini L et al. (2011). Sea-bottom observations from the western escarpment of the Sea of Marmara. Bulletin of the Seismological Society of America 101: 2. http://doi.org/10.1785/012000014

Tüysüz O, Barka AA, Yiğitbaş E (1998). Geology of the saros graben: its implications on the evolution of the North Anatolian Fault in the Ganos-Saros region, NW Turkey. Tectonophysics 293: 105–126.

Vannucci G, Gasperini P (2003). A database of revised fault plane solutions for Italy and surrounding regions. Computers & Geosciences 29: 903-909.

Wessel P, Smith WHF (1991). Free software helps map and display data. Eos Transactions of the American Geophysical Union 72: 441. https://doi.org/10.1029/90EO00319

Wilson JT (1965). A new class of faults and their bearing on continental drift. Nature 207: 343–347.

Yaltırak C, Sakınç M, Oktay FY (2000). Westward propagation of the North Anatolian fault into the northern Aegean: timing and kinematics. Geology 28, 187-188.

Yamamoto Y, Takahashi N, Citak S, Kalafat D, Pinar A et al. (2015). Offshore seismicity in the western Marmara Sea, Turkey, revealed by ocean bottom observation. Earth, Planets and Space 67: 147. http://doi.org/10.1186/s40623-015-0325-9

Yamamoto R, Kido M, Ohta Y, Takahashi N, Yamamoto Y et al. (2019). Seafloor geodesy revealed partial creep of the North Anatolian Fault submerged in the Sea of Marmara. Geophysical Research Letters 46 (3): 1268–1275.

Yamamoto Y, Kalafat D, Pinar A, Takahashi N, Coskun Z et al. (2020). Fault geometry beneath the western and Central Marmara Sea, Turkey, based on ocean bottom seismographic observations: Implications for future large earthquakes. Tectonophysics 791: 228568.

Supplementary Table 1. Source parameters of 99 events obtained by CMT inversion method.

Event number	Location	Date	Time	Latitude	Longitude	M_W	H	Strike	Dip	Rake
1	Asmalı-Balıkesir-Marmara Sea	19.04.2004	15.27	40.61	27.70	3.7	15	101	69	135
2	Gulf of İzmit	16.05.2004	03:30	40.72	29.33	4.3	3	94	72	–111
3	Çınarcık Offshore-Yalova	29.09.2004	15:42	40.79	29.02	3.8	6	85	67	82
4	Gulf of Gemlik-Marmara Sea	24.10.2006	14:00	40.42	28.99	4.9	9	97	45	–88
5	Samanlı-Yalova	28.10.2006	15:28	40.64	29.23	3.4	6	248	72	–119
6	Şenköy-Çınarcık	12.03.2008	18:53	40.62	29.01	4.4	9	89	78	–129
7	Şenköy-Çınarcık	05.10.2008	06:04	40.63	29.01	3.8	9	89	51	–117
8	Yalova Offshore-Marmara Sea	22.10.2008	01:00	40.74	29.17	3.7	3	110	70	–154
9	Ericek-Bolu	12.11.2008	11:57	40.78	31.92	3.9	12	251	71	135
10	Aşağıkuzören-Bolu	12.11.2008	14:25	40.81	31.96	3.7	9	251	73	123
11	Kozlu-Bolu	16.08.2010	03:09	40.83	31.58	3.7	3	83	89	179
12	Tuzla-Marmara Sea	09.05.2011	03:01	40.85	29.29	3.2	6	281	63	–121
13	Kızılağıl-Bolu	13.05.2011	22:28	40.77	31.53	3.9	4	302	66	–160
14	Marmara Sea	25.07.2011	17:57	40.81	27.74	4.9	6	255	81	153
15	Kaleköy-Gökçeada	31.07.2013	01:26	40.31	25.80	3.8	9	238	86	–157
16	Biga-Çanakkale	29.08.2013	06:20	40.35	27.45	3.9	12	66	65	172
17	Şarköy-Tekirdağ	25.09.2013	13:39	40.77	27.42	3.2	10	241	53	124
18	Gulf of Saros-Aegean Sea	25.10.2013	12:01	40.41	26.06	3.6	9	119	35	–97
19	Aegean Sea	23.11.2013	10:27	40.58	25.69	3.6	10	96	39	–91
20	Ulumescit-Bolu	24.11.2013	20:49	40.78	31.88	4.7	6	74	27	110
21	Gelibolu-Çanakkale	22.04.2014	18:27	40.46	26.46	3.3	6	77	30	–81
22	Gulf of Saros-Aegean Sea	24.05.2014	15:01	40.38	26.14	3.9	9	66	37	–101
23	Aegean Sea	24.05.2014	16:34	40.29	25.63	3.8	9	93	64	–94
24	Gulf of Saros-Aegean Sea	25.05.2014	01:50	40.40	25.92	3.5	6	107	57	–106
25	Gulf of Saros-Aegean Sea	25.05.2014	05:44	40.42	26.07	3.9	9	102	60	–108
26	Gulf of Saros-Aegean Sea	25.05.2014	11:47	40.41	26.09	4.2	2	79	40	171
27	Kaleköy-Gökçeada	27.05.2014	11:42	40.36	25.88	3.5	8	80	87	166
28	Gulf of Saros-Aegean Sea	28.05.2014	03:59	40.42	26.13	4.3	6	80	12	–111
29	Termal-Yalova	03.08.2014	10:42	40.61	29.16	3.5	4	109	41	–70
30	Termal-Yalova	03.08.2014	22:22	40.61	29.17	3.9	3	118	43	–62
31	Şarköy-Marmara Sea	04.11.2005	20:12	40.68	27.30	3.7	6	202	52	110
32	Şarköy-Marmara Sea	18.08.2007	07:37	40.64	27.25	3.4	3	99	76	–136
33	Biga-Çanakkale	12.04.2008	03:25	40.38	27.42	3.4	12	273	86	165
34	Şarköy-Marmara Sea	14.07.2008	16:02	40.74	27.36	3.3	10	56	70	110
35	Marmara Sea	23.01.2009	16:34	40.79	27.77	3.5	15	163	36	–140
36	Marmara Sea	18.03.2009	16:33	40.80	27.76	3.8	9	277	74	175
37	Marmara Sea	27.04.2009	19:03	40.73	27.53	4.0	12	261	43	–160
38	Marmara Sea	25.10.2009	03:26	40.79	27.76	3.6	12	144	41	–124
39	Çınarcık Offshore-Yalova	23.06.2002	23.09	40.76	29.03	2.7	3	340	66	–78
40	Çınarcık Offshore-Yalova	22.07.2003	23:55	40.73	29.07	3.0	2	110	45	–137
41	Çiftlikköy-Yalova	16.05.2004	21:07	40.70	29.31	3.3	5	100	48	–128

Supplementary Table 1. (Continued).

42	Çınarcık Offshore-Yalova	29.09.2004	15:51	40.78	29.04	2.7	20	291	57	–163
43	Çınarcık Offshore-Yalova	14.08.2005	21:11	40.74	29.04	3.4	4	315	58	–97
44	Çınarcık Offshore-Yalova	07.09.2005	13:22	40.73	29.22	3.3	9	281	70	–135
45	Çınarcık Offshore-Yalova	07.09.2005	13:50	40.74	29.25	3.2	9	290	48	–127
46	Çınarcık-Yalova	26.11.2005	22:27	40.65	29.07	3.2	6	292	56	–109
47	Çınarcık-Yalova	18.08.2008	11:06	40.71	29.12	3.0	12	248	56	–175
48	Çınarcık-Yalova	18.08.2008	11:08	40.72	29.12	3.1	10	265	64	–160
49	Çınarcık Offshore-Yalova	21.02.2009	22:29	40.76	29.05	3.3	6	303	53	–112
50	Çınarcık Offshore-Yalova	21.02.2009	23:04	40.73	29.02	3.4	6	294	63	–111
51	Koru-Çınarcık-Yalova	12.07.2009	06:59	40.67	29.17	3.3	8	253	36	–120
52	Şenköy- Çınarcık-Yalova	16.11.2009	18:47	40.60	29.01	3.2	12	88	41	–140
53	Marmara Sea	14.03.2012	09:25	40.81	28.79	3.7	10	347	49	–124
54	Lapseki-Çanakkale	04.05.2012	05:38	40.310	27.00	3.9	6	273	45	–162
55	Biga-Çanakkale	16.12.2014	09:02	40.149	27.083	4.1	12	261	85	174
56	Kuş Lake-Balıkesir	03.07.2014	05:04	40.208	27.933	4.3	9	79	86	147
57	Manyas-Balıkesir	30.03.2011	17:07	40.048	27.831	4.0	12	81	76	177
58	Gulf of Bandırma	09.03.2011	07:04	40.431	28.059	3.8	9	75	77	–120
59	Bayraktar-İzmit	01.08.2007	19:03	40.786	30.090	3.7	12	91	57	113
60	Enez-Edirne	20.05.2011	22:34	40.881	26.003	3.4	6	99	79	–176
61	Geyve-Sakarya	22.10.2014	17:11	40.406	30.114	4.2	6	66	38	–161
62	Kaynaşlı-Düzce	07.07.2015	05:08	40.820	31.291	3.7	15	322	70	–120
63	İnhisar-Bilecik	28.06.2014	01:39	40.085	30.385	3.8	6	210	30	–149
64	Tekirdağ Offshore-Marmara	01.02.2015	10:46	40.696	27.505	3.0	6	67	61	128
65	Biga-Çanakkale	16.12.2014	09:03	40.156	27.086	3.5	20	76	67	163
66	Mustafakemalpaşa-Bursa	23.01.2015	10:19	40.065	28.590	4.2	2	67	44	–135
67	Akyazı-Sakarya	31.05.2004	22:50	40.510	30.600	3.7	15	96	38	–101
68	Asmalı-Balıkesir	16.01.2005	09:57	40.609	27.723	3.2	9	246	77	–155
69	Gulf of Saros-Aegean Sea	09.04.2005	19:28	40.484	25.814	3.6	6	186	76	115
70	Biga-Çanakkale	27.07.2014	14:09	40.178	26.891	3.4	12	192	85	150
71	Aegean Sea	28.05.2014	10:31	40.282	25.482	3.5	9	30	68	–177
72	Güzelköy Offshore-Tekirdağ	27.06.2005	02:58	40.692	27.387	3.4	6	121	23	–129
73	Mürefte Offshore-Tekirdağ	01.06.2014	21:17	40.561	27.334	3.2	6	250	72	–172
74	Engurucuk-Gemlik	11.05.2015	04:16	40.415	29.125	3.5	8	265	59	–121
75	Kaleköy-Gökçeada	26.05.2014	18:54	40.400	25.894	3.5	10	272	79	–87
76	Gulf of Gemlik-Marmara Sea	27.10.2012	02:37	40.435	28.727	3.7	6	257	65	–130
77	Kaleköy-Gökçeada	30.07.2013	06:28	40.302	25.774	3.8	9	241	59	–156
78	Gulf of Gemlik-Marmara Sea	26.10.2012	03:37	40.425	28.720	3.6	9	251	75	–155
79	Güzelköy Offshore-Tekirdağ	27.03.2005	09:32	40.737	27.408	3.5	9	250	80	159
80	Aegean Sea	30.05.2014	05:21	40.188	25.554	3.6	6	224	87	–119
81	Gölyaka-Düzce	13.09.2004	01:48	40.790	30.990	3.4	2	230	15	–108
82	Gulf of Saros	17.06.2004	12:48	40.490	26.110	2.8	9	112	62	–119
83	Gulf of Gemlik-Marmara Sea	11.10.2004	01:25	40.430	28.940	3.6	20	253	48	–164
84	Kocadere-Çanakkale	24.07.2015	01:26	40.242	26.302	4.3	4	33	88	168

Supplementary Table 1. (Continued).

85	Kumbağ-Tekirdağ	13.07.2003	05:09	40.830	27.400	3.6	20	229	55	129
86	Kuş Lake	09.06.2003	17:44	40.210	27.940	4.4	12	263	90	–138
87	Güzelköy Offshore-Tekirdağ	20.08.2005	06:09	40.760	27.425	3.5	20	40	76	168
88	Akyazı-Sakarya	17.09.2002	12:05	40.720	30.610	3.8	16	262	52	–110
89	Biga-Canakkale	03.06.2008	06:59	40.163	26.918	3.5	9	116	61	133
90	Marmara Sea	03.10.2010	17:49	40.840	28.140	4.1	9	79	86	–178
91	Mürefte Offshore-Tekirdağ	12.05.2008	15:11	40.634	27.373	3.6	18	273	82	161
92	Marmara Ereğlisi Offshore-Tekirdağ	12.08.2008	15:41	40.834	27.956	3.3	6	93	74	–161
93	Marmara Sea	24.01.2009	15:58	40.785	27.764	4.0	9	137	36	–119
94	Marmara Sea	25.07.2011	20:43	40.816	27.733	3.6	5	247	78	–169
95	Marmara Ereğlisi Offshore-Tekirdağ	07.06.2012	20:54	40.854	27.923	4.9	5	89	85	173
96	Marmara Ereğlisi Offshore-Tekirdağ	12.08.2008	15:41	40.834	27.856	3.0	9	113	78	–175
97	Marmara Ereğlisi Offshore-Tekirdağ	27.11.2013	04:13	40.845	27.918	4.6	5	86	77	171
98	Marmara Sea	28.10.2015	16:20	40.820	27.764	4.3	6	246	69	160
99	Aegean Sea	24.05.2014	09:25	40.290	25.400	6.8	18	76	85	173

H = CMT depth in km.

Supplementary Table 2. Focal mechanism parameters derived from simultaneous inversion of the polarity data acquired in Ganos Area.

Event number	Date	Time	Lat.	Lon.	M_W	H	Strike	Dip	Rake	Number of stations
1	18.04.2013	19:36	40.75	27.40	3.0	9.8	27	50	–32	23 land stations
2	28.07.2013	17:45	40.76	27.45	2.9	15.7	12	40	31	25 land stations
3	17.08.2013	03:37	40.76	27.42	3.1	8.7	70	45	–111	17 land stations
4	25.09.2013	13:39	40.77	27.42	3.5	7.5	5	33	27	24 land stations
5	08.12.2013	03:51	40.75	27.38	2.8	15.0	336	27	–67	16 land stations
6	22.02.2014	22:45	40.78	27.45	3.2	14.3	301	22	–42	16 land stations
7	11.04.2014	12:59	40.80	27.51	3.0	13.3	324	50	–26	17 land stations
8	27.04.2014	07:13	40.77	27.36	3.1	8.6	232	68	169	24 land stations
9	04.05.2014	12:45	40.77	27.37	2.7	7.3	358	34	27	12 land stations
10	19.06.2014	21:14	40.65	27.53	2.9	8.7	10	44	–16	22 land stations
11	20.06.2014	22:21	40.71	27.47	2.8	9.1	90	35	–156	22 land stations
12	17.09.2014	12:20	40.78	27.42	2.7	16.2	261	55	–159	13 land stations
13	07.10.2014	23:49	40.78	27.56	2.8	12.4	337	47	–60	21 land stations
14	08.10.2014	03:08	40.76	27.49	3.3	19.2	261	55	–159	24 land stations
15	23.10.2014	14:53	40.74	27.39	3.4	8.7	120	45	–126	21 land stations
16	03.12.2014	05:39	40.73	27.31	2.8	10.7	292	17	–35	13 land stations
17	01.02.2015	10:46	40.70	27.51	3.5	5.6	331	41	–60	19 land stations
18	04.10.2015	00:24	40.75	27.38	3.0	16.6	255	79	180	21 land stations
19	25.10.2015	15:58	40.80	27.43	2.7	14.9	340	45	–22	11 OBS+15 land stations
20	04.12.2015	06:52	40.74	27.44	2.9	7.1	324	50	–26	11 OBS+13 land stations
21	07.12.2015	12:02	40.71	27.43	3.3	5.2	358	34	27	12 OBS+22 land stations
22	26.12.2015	22:31	40.68	27.46	2.7	9.4	337	47	–60	15 land stations
23	19.01.2016	13:09	40.72	27.43	2.6	7.6	299	26	–50	6 OBS+11 land stations
24	19.01.2016	13:10	40.71	27.42	2.4	9.8	135	20	173	4 OBS+10 land stations
25	11.02.2016	01:53	40.56	27.34	3.4	14.1	75	35	–160	27 land stations
26	15.04.2016	09:05	40.79	27.47	3.1	13.8	330	33	28	11 OBS+21 land stations
27	26.07.2015	06:47	40.88	27.55	2.8	16.1	54	32	52	14 OBS stations
28	05.08.2015	06:31	40.76	27.36	2.7	12.2	150	30	–159	11 OBS stations
32	04.09.2015	13:18	40.72	27.40	2.4	9.7	292	40	–61	10 OBS stations
59	28.11.2015	03:10	40.82	27.43	2.0	12.1	270	10	–82	10 OBS stations
61	30.11.2015	16:09	40.77	27.47	2.7	15.3	45	20	46	10 OBS stations
62	03.12.2015	03:27	40.86	27.47	2.3	13.2	49	21	45	10 OBS stations
63	07.12.2015	20:57	40.70	27.35	3.9	11.3	89	5	103	13 OBS stations
68	06.10.2016	19:12	40.87	27.42	2.6	9.3	337	40	–24	10 OBS stations
70	16.11.2016	21:33	40.72	27.41	2.4	9.4	305	50	–37	10 OBS stations
89	28.03.2016	17:23	40.74	27.50	4.1	16.2	90	20	123	13 OBS stations
94	02.05.2016	12:21	40.72	27.37	2.0	8.4	135	20	173	10 OBS stations

Supplementary Table 3. Focal mechanism parameters derived from simultaneous inversion of the polarity data acquired in Western Marmara Segment.

Event number	Date	Time	Lat.	Lon.	M_W	H	Strike	Dip	Rake	Number of stations
30	29.08.2015	12:47	40.87	27.92	3.9	15.4	287.2	75.5	–174.9	12 OBS stations
31	29.08.2015	18:14	40.86	27.92	2.2	14.2	315.1	10.0	–67.3	11 OBS stations
33	13.09.2015	05:11	40.80	27.68	2.3	17.6	17.0	54.6	18.5	10 OBS stations
35	19.09.2015	18:49	40.80	28.02	2.4	17.9	120.0	15.0	136.1	10 OBS stations
36	01.10.2015	10:45	40.84	27.71	2.6	19.3	0.0	40.0	–37.6	10 OBS stations
38	16.10.2015	02:00	40.80	27.79	2.3	18.8	165.0	30.0	–131.7	11 OBS stations
39	28.10.2015	16:20	40.83	27.73	4.6	14.6	348.0	75.0	–5.6	13 OBS stations
40	28.10.2015	16:22	40.84	27.75	2.7	11.6	108.0	25.0	–156.4	10 OBS stations
41	28.10.2015	18:43	40.83	27.72	2.1	12.1	315.1	30.0	–72.5	10 OBS stations
42	28.10.2015	21:50	40.82	27.72	2.2	12.1	10.6	17.8	–16.6	11 OBS stations
44	02.112015	10:33	40.53	27.96	1.9	13.8	112.5	20.0	156.5	10 OBS stations
45	02.11.2015	18:32	40.84	27.73	2.2	19.9	276.9	65.0	–176.3	10 OBS stations
46	10.11.2015	11:23	40.80	27.89	2.2	14.5	298.7	21.3	–45.3	11 OBS stations
47	01.11.2015	11:26	40.79	27.89	2.8	16.0	85.3	53.5	–141.5	12 OBS stations
58	25.11.2015	09:34	40.80	27.89	1.8	14.1	283.8	65.0	–170.3	10 OBS stations
60	28.11.2015	06:41	40.79	27.90	3.2	16.2	0.0	80.0	–2.9	12 OBS stations
64	22.12.2015	15:10	40.83	27.76	2.8	17.3	276.4	70.0	160.6	12 OBS stations
65	03.01.2016	17:46	40.74	28.05	2.9	15.9	90.0	20.0	76.4	11 OBS stations
66	06.10.2016	15:44	40.73	28.05	3.3	16.5	337.4	40.0	–52.1	13 OBS stations
67	06.10.2016	16:04	40.73	28.05	3.0	16.9	330.9	42.8	–71.2	12 OBS stations
69	12.01.2016	01:48	40.83	27.73	3.1	12.2	283.7	27.7	–65.3	13 OBS stations
71	28.01.2016	15:06	40.76	28.08	2.5	16.0	337.4	40.0	–52.1	13 OBS stations
72	30.01.2016	09:03	40.76	28.07	3.8	16.9	100.0	45.0	–108.7	13 OBS stations
74	01.02.2016	18:38	40.76	28.08	2.9	16.1	345.0	30.0	–47.3	11 OBS stations
78	24.02.2016	04:26	40.85	27.71	2.2	20.4	0.0	80.0	–2.9	12 OBS stations
79	29.02.2016	04:52	40.83	28.15	2.2	13.8	257.1	70.0	159.6	11 OBS stations
80	01.03.2016	14:54	40.86	27.75	2.7	22.0	275.0	72.5	180.0	13 OBS stations
81	10.03.2016	14:47	40.82	28.07	2.5	16.6	315.4	38.7	–66.5	11 OBS stations
82	11.03.2016	18:40	40.82	28.08	2.2	15.7	360.0	75.1	–13.2	12 OBS stations
83	23.03.2016	03:51	40.86	27.95	3.1	17.2	263.6	70.0	159.8	12 OBS stations
84	24.03.2016	08:04	40.85	27.95	3.7	18.0	270.0	60.0	–160.2	13 OBS stations
85	25.03.2016	22:18	40.85	27.99	2.2	16.6	348.0	75.0	–5.6	10 OBS stations
86	27.03.2016	05:03	40.83	27.87	3.2	23.4	360.0	55.0	–33.9	13 OBS stations
87	27.03.2015	05:03	40.83	27.87	3.9	22.5	360.0	50.0	–35.9	11 OBS stations
88	27.03.2016	05:05	40.82	27.86	2.5	22.0	15.1	30.0	–27.8	10 OBS stations
90	01.04.2016	23:22	40.85	27.97	2.3	24.4	208.1	80.0	6.2	12 OBS stations
91	06.04.2016	04:34	40.87	27.91	2.5	14.5	296.5	68.1	–169.2	12 OBS stations
100	05.06.2016	20:49	40.85	27.94	2.2	17.0	210.1	15.0	–149.1	11 OBS stations

Supplementary Table 4. Focal mechanism parameters derived from simultaneous inversion of the polarity data acquired in Central Marmara Segment.

Event number	Date	Time	Lat.	Lon.	M_W	H	Strike	Dip	Rake	Number of stations
29	24.08.2015	04:47	40.83	28.27	2.6	5.3	337	20	–10	10 OBS stations
34	17.09.2015	21:39	40.84	28.30	2.3	6.9	90	25	–171	10 OBS stations
43	31.10.2015	21:10	40.86	28.78	2.8	11.9	180	22	180	10 OBS stations
48	16.11.2015	15:45	40.89	28.76	4.2	11.6	146	40	–161	14 OBS stations
49	16.11.2015	16:36	40.90	28.74	3.2	10.3	157	20	–176	12 OBS stations
50	16.11.2015	17:04	40.90	28.76	3.7	9.4	215	40	–83	14 OBS stations
51	16.11.2015	18:13	40.90	28.74	2.9	9.0	144	25	–178	11 OBS stations
52	17.11.2015	02:17	40.89	28.77	3.3	9.4	230	45	–128	12 OBS stations
53	17.11.2015	03:05	40.92	28.74	2.5	9.4	228	40	–80	10 OBS stations
54	17.11.2015	04:36	40.89	28.74	3.4	12.2	180	50	–169	11 OBS stations
55	18.11.2015	12:52	40.87	28.76	3.4	12.3	150	45	–158	13 OBS stations
73	30.01.2016	16:33	40.83	28.27	2.5	5.2	22	20	22	11 OBS stations
75	05.02.2016	08:02	40.83	28.34	3.2	11.7	110	45	–87	13 OBS stations
76	12.02.2016	17:43	40.85	28.55	2.5	7.9	15	30	–6	12 OBS stations
77	19.02.2016	10:37	40.90	28.67	2.5	8.6	249	65	179	11 OBS stations
92	25.04.2016	01:51	40.83	28.42	1.9	6.8	360	40	–20	10 OBS stations
93	27.04.2016	12:07	40.41	28.68	3.6	11.7	254	29	–159	10 OBS stations
95	31.05.2016	21:14	40.84	28.23	3.4	7.5	359	25	1	13 OBS stations
96	31.05.2016	21:17	40.85	28.23	2.2	7.3	0	30	–4	11 OBS stations
97	01.06.2016	12:32	40.84	28.23	2.3	7.1	340	45	–13	11 OBS stations
98	02.06.2016	03:56	40.84	28.24	2.3	7.4	330	15	–15	10 OBS stations
99	03.06.2016	03:06	40.85	28.23	2.4	7.6	342	50	–14	12 OBS stations
101	15.06.2016	05:20	40.84	28.23	3.5	7.0	110	45	–87	12 OBS stations
102	17.06.2016	06:35	40.84	28.23	2.3	7.0	18	25	8	10 OBS stations